Electronic Supplementary Information (ESI) for Green Chemistry
This journal is (c) The Royal Society of Chemistry 2012

Electronic Supplementary Information

Surface dealloyed PtCo nanoparticles supported on carbon nanotube: facile synthesis and promising application for anion exchange membrane direct crude glycerol fuel cell

Ji Qi,[a] Le Xin,[a] Zhiyong Zhang,[a] Kai Sun,[b] Haiying He,[c] Fang Wang,[a] David Chadderdon,[a] Yang Qiu, [a] Changhai Liang[d] and Wenzhen Li*[a]

[a] *Department of Chemical Engineering, Michigan Technological University, Houghton, Michigan, USA. Fax: +1-906-487-3213; Tel: +1-906-487-2298; E-mail: wzli@mtu.edu*

[b] *Department of Materials Science and Engineering, University of Michigan, Ann Arbor, USA.*

[c] *Department of Physics, Michigan Technological University, Houghton, Michigan, USA.*

[d] *School of Chemical engineering, Dalian University of Technology, Dalian, Liaoning, China.*

Comparison of different alcohol fuel from price and performance aspects

The average price of crude glycerol is only \$0.82 gal^{-1}, which is 81.4%, 38.8%, 74.0% lower than that of refined glycerol, methanol and ethanol, respectively. However, the performance of direct crude glycerol AEMFC is comparable to (only 5.65% lower than) that of direct high purity glycerol AEMFC.

Tab. S1 Alcohol fuel price and published results of highest DAFC performances.

	Price in North America	Highest performance of AEMFC (low T <100℃)	Highest performance of PEMFC (low T <100℃)	Highest performance of SOFC (high T >500℃)
Crude Glycerol (a minimum 85% glycerol, with low salts and MONG (many organics not glycerol))	0.74-0.89 dollars gal^{-1} Ref [1]	Results of this paper 268.5 mW cm^{-2} (0.5 mg_{Pt} cm^{-2}, 80 ℃, O_2) 200 mW cm^{-2} (0.5 mg_{Pt} cm^{-2}, 80 ℃, air)	Not available	Not available
Refined Glycerol	4.00–4.84 dollars gal^{-1} Ref [1]	124.5 mW cm^{-2} (1 mg_{Pt} cm^{-2} , 80℃, O_2) [2] Results of this paper 284.6 mW cm^{-2} (0.5 mg_{Pt} cm^{-2}, 80℃, O_2)	Not available	327 mW cm^{-2} (800℃) [3] 215 mW cm^{-2} (580℃) [4]
Methanol	1.45 dollars gal^{-1} Ref [5]	168 mW cm^{-2} (3.0 mg_{PtRu} cm^{-2} 90℃, O_2)[6]	246 mW cm^{-2} (90℃) [7]	1600 mW cm^{-2} (750℃) [8]
Ethanol	2.39 dollars gal^{-1} Ref [9]	185 mW cm^{-2} (1.2 mg_{PdAu} cm^{-2} 60℃ using O_2) [10] 240 mW cm^{-2} (1 mg_{Pd} cm^{-2}, 60℃, using H_2O_2) [11]	79.5 mW cm^{-2} (90℃) [12]	800 mW cm^{-2} (800℃) [13] 160 mW cm^{-2} (580℃) [13]

AEMFC: Anion exchange membrane fuel cell

PEMFC: Proton exchange membrane fuel cell

SOFC: Solid oxide fuel cell

Chemicals

Sodium borohydride ($NaBH_4$, 99%) and high purity glycerol (99%) were purchased from Acros Organics. Carboxyl group functionalized multiwall carbon nanotube (CNT) was obtained from Cheaptubes Inc. Chloroplatinic acid hydrate (H_2PtCl_6, 37%-40% Pt) and cobalt chloride hexahydrate ($CoCl_3$, 98%) were bought from Sigma-Aldrich Co. Crude glycerol (a byproduct from soy biodiesel manufacturing, 88.05 wt% of glycerol, 5.42 wt% of matter organic non glycerol (MONG), 4.16 wt% of moisture, 2.37 wt% of ash, and 628 ppm methanol) was provided by Kingdom Bio Solutions Inc. All the chemicals were used as received without further purification.

Synthesis of surface dealloyed PtCo supported on carbon nanotube

Chloroplatinic acid hydrate (130.1 mg) and cobalt chloride hexahydrate (59.6 mg) were mixed together with carboxyl group functionalized multiwall carbon nanotube (180.3.0 mg) in 500 ml ethanol, followed by 30 minutes ultrasonic treatment, so as to ensure that all of them are well-dispersed. After that, the mixture was kept in ice water for 5 minutes, which would prevent it from becoming too hot during the subsequent reduction process. Sodium borohydride (360 mg) was dissolved in ethanol (100 ml) and then blended with the above mixture to reduce metal precursors and deposit the PtCo nanoparticles onto the surface of CNT After filtrating and washing with 300ml deionized water and ethanol mixed solution (1:4 in volume), the PtCo/CNT was collected and dried in vacuum oven under 50℃ overnight. PtCo/CNT powder (100 mg) was then re-dispersed into 300 ml ethanol by 10 minutes ultrasonic treatment. 0.5 M hydrochloric acid (400 ml) in ethanol was added to the mixture to process the surface dealloy treatment. The SD-PtCo/CNT was finally obtained by filtration, washing with 200 ml ethanol, and dried in vacuum oven under 50 ℃ overnight. Pt/CNT was synthesized via a similar process as the PtCo/CNT. All the catalysts in the experiment were controlled to have a Pt loading of 20%.

Structure and morphology characterization

The structure, composition and morphology of Pt/C, Pt/CNT, SD-PtCo/CNT catalysts were characterized by X-ray diffraction (XRD), inductively coupled plasma atomic emission spectroscopy (ICP-AES), transmission election microscopy (TEM) and high angle annular dark field scanning transmission electron microscopy (HAADF-STEM). XRD patterns were collected by a Scintag XDS-2000 θ/θ diffractometer using Cu Kα radiation (λ = 1.5406 Å) with a filament current of 35 mA and a tube voltage of 45 kV. TEM was performed on JEOL JEM-4000FX, operated at voltage of 200 kV. JEOL 2010F operated at 200 kV was used for HAADF imaging. The catalysts were dissolved in aqua regia solution (‘royal water’) over night before conducting ICP-AES test.

Half-cell test

A conventional three-electrode, water jacket integrated glass cell (AFCELL3, Pine Instrument) with a glassy carbon working electrode (AFE3T050GC, Pine Instrument), a Hg/HgO reference electrode (MMO, CHI152, CH Instruments), and a Pt wire counter electrode (AFCTR1, Pine Instrument), were used for cyclic voltammetry (CV) and linear scan voltammetry (LSV) experiments of the commercial Pt/C (Etek), as-prepared Pt/CNT and SD-PtCo/CNT catalysts at room temperature. Unless specified otherwise, all potentials in the present research were referred to MMO (1.0 M KOH, 0.098 V vs. SHE). Uniformly dispersed catalysts ink with a concentration of 1 mg mL^{-1} was obtained by ultrasonically treating a mixture of 2.0 mL iso-propanol and 2.0 mg catalysts in ice-water bath for 10 minutes. After polishing the glassy carbon electrode (GCE) with alumina micropolish solution and grinding paper, 5 μl of the ink was dropwise added and evenly distributed on the surface of GCE. The electrolyte solution was under 99.999% high purity N_2 protection during the whole experimental process. The scan rate is 50 mV s^{-1} for CV test, and 1 mV s^{-1} for LSV test.

Single cell test

A fuel cell test system (850e Scribner-Associates) with self-made membrane electrode assembly (MEA), serpentine graphite flow field plate, and feedback temperature control loop composed of electric heating rods and thermocouple thermometer, was used to obtain polarization curve, power density curve and single cell inner resistance. The MEA with an active area of 5 cm^2 was composed of carbon cloth as anode catalyst substrate, anion exchange membrane (A901 Tokuyama, 10 μm), carbon paper as cathode backing layer. The anode catalyst substrate, obtained by spraying catalyst ink onto carbon cloth, had a 0.5 mg cm^{-2} metal loading of Pt/C, Pt/CNT, or SD-PtCo/CNT catalyst. Before spraying, the catalyst ink with 15 mg cm^{-3} concentration, utilizing iso-propanol as solvent and 5% polytetrafluoroethylene (PTFE Teflon® DuPont) as binder (catalyst: PTFE = 9:1 mass ratio), was ultra-sonicated in ice-water bath for 30 min to ensure uniform dispersion. The cathode is prepared by spraying a mixture (catalyst: ionomer = 7:3 mass ratio) of 3.5 wt% non-noble metal loading commercial catalyst (4020 Acta) and ionomer (AS-4 Tokuyama) onto an anion exchange membrane (A901 Tokuyama), subsequently followed by covering a carbon paper as the cathode backing layer.

Glycerol conversion analysis

High-performance liquid chromatography (HPLC, Agilent 1100) with a refractive index detector (RID), a variable wavelength detector (VWD) and an OA-1000 column (Alltech) was employed to quantify the conversion of glycerol in active direct glycerol fuel cell operated at different potentials. The temperature of column was 60 ℃. 5 mM H_2SO_4 was used as mobile phase with a flow rate of 0.3 mL min^{-1}. The sample volume was controlled to be 20 μL.

Particle size and lattice constant calculation based on XRD characterization

The XRD patterns of Pt/C (Etek), Pt/CNT and SD-PtCo/CNT catalysts are shown in Fig 2(E) in the main article, which indicates that the metal particles have the face-centered cubic (FCC) structure. Typical for nanosized materials, the diffraction peaks are fairly board. The mean crystallite size of Pt/C (Etek), PtCo/CNT and SD-PtCo/CNT catalysts are calculated using the (220) peak based on Debye-Scherrer formula, while lattice constants for Pt/C (Etek), PtCo/CNT and SD-PtCo/CNT catalysts are calculated using the (220) peak based on the combination of Bragg's law and the relationships between lattice constant and crystal lattice spacing :

$$L = \frac{0.9\lambda_{K\alpha}}{B_{2\theta}\cos\theta_{max}}$$

$$a_{fcc} = \frac{\sqrt{2}\lambda_{K\alpha}}{\sin\theta_{max}}$$

Where L is the mean crystallite size, $\lambda_{K\alpha}$ is the wavelength of the X-ray (1.5406 Å), B is the full width at half-maximum (FWHM) of the peak (rad), θ_{max} is the Bragg angle (rad) of (220) peak position, and a_{fcc} is the lattice constant for fcc structure. According to the above-mentioned equation, the mean crystallite size of the metal particles on the Pt/C (Etek), Pt/CNT , PtCo/CNT and SD-PtCo/CNT catalyst is 1.9 nm, 2.9 nm, 2.1 nm, 2.2 nm while the lattice constant of them is 3.944 Å, 3.918 Å, 3.834 Å, 3.808 Å, respectively.

Catalyst loading and atomic ratio determined by ICP-AES

The Pt loading of PtCo/CNT (before dealloy treatment) and SD-PtCo/CNT (after dealloy treatment) is 19.3% and 19.1%, respectively, indicating that the metal precursors have been fully reduced. The Pt: Co atomic ratio of PtCo/CNT and SD-PtCo/CNT is 53:47 and 69:31, respectively, suggesting that most of the surface Co atoms of the catalyst had been removed by the dealloy treatment.

Direct crude glycerol fuel cell operated under different conditions

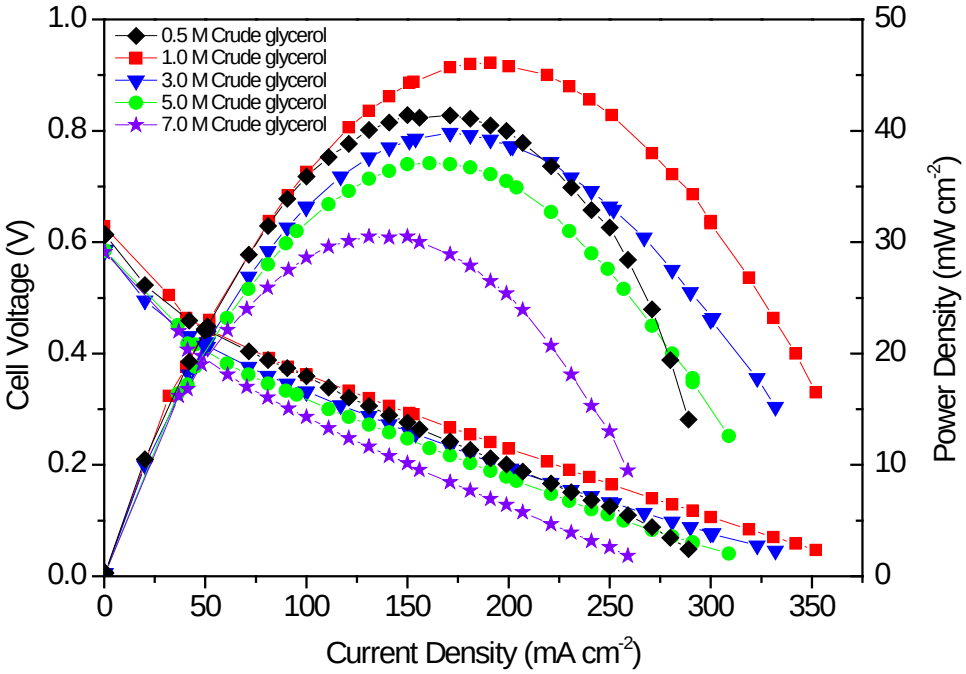

Fig. S1 Polarization and power density curves of direct crude glycerol/O_2 AEMFC with SD-PtCo/CNT as anode catalyst using different crude glycerol concentrations. Anode catalyst (0.5 mg_{Pt} cm^{-2}): SD-PtCo/CNT (Self-prepared); anion exchange membrane: Tokuyama A901; cathode catalyst (3.0 $mg_{catalyst}$ cm^{-2}): Fe-Cu-N_4/C (Acta 4020); anode fuel: 1.0 M KOH, 1.0 ml min^{-1}; cathode fuel: 100 sccm O_2, ambient pressure; temperature (anode fuel/cathode fuel/cell): 25/60/60 ℃.

Fig. S1 presents the crude glycerol concentration effects on polarization and power density curves of direct crude glycerol/O_2 AEMFC with SD-PtCo/CNT as anode catalyst. When crude glycerol concentration is > 1.0 M, cell voltage loss increases with crude glycerol concentration increasing in all the current region. The first reason can be attributed to the increment of single cell internal resistance, as presented in Fig. S2. In view of crude glycerol's high viscosity, increment of its concentration will remarkably increase the viscosity of fuel solution, which will lower the mobility of anion and cation, and reduce the conductivity of the electrolyte, so that the single cell internal resistance increases. The second reason is linked to the depression of glycerol oxidation kinetics, as indicated by the OCV drop along with glycerol concentration accretion manifested in Fig. S2. On one hand, the hydroxyl anion's mass transfer issue, emerged as crude glycerol concentration increases, will result in its concentration drop inside the anode catalyst layer. On the other hand, the amount of adsorbed hydroxyl anion on the catalyst active sites will decrease when glycerol concentration is higher due to the competitive adsorption between hydroxyl anion and glycerol. To sum up, when the crude glycerol concentration increases from 1.0 M to 7.0 M, single cell performance will decrease in all the current region.

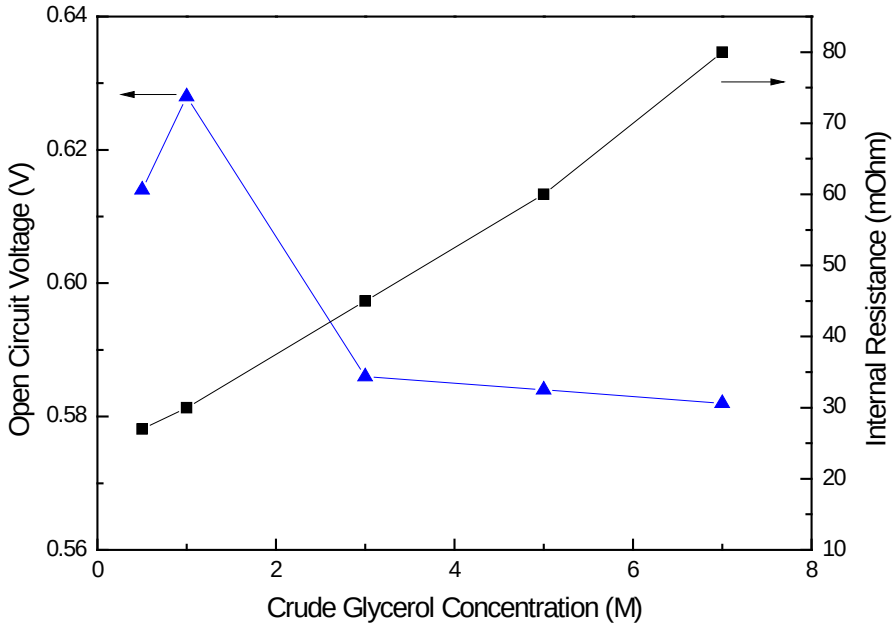

Fig. S2 The effect of crude glycerol concentration on open circuit voltage and internal resistance.

When crude glycerol concentration changes from 0.5 M to 1.0 M, cell voltage is slightly increased in the low current region and is markedly increased in high current region. In the low current region, the oxidation rate of glycerol is relative slow, wherefore 0.5 M and 1.0 M crude glycerol are all adequate to maintain an appropriate concentration in the anode catalyst layer at 1.0 M KOH. However, in the high current region, faster oxidation rate of glycerol will lead to insufficient supply of reagent glycerol. Meanwhile under relatively low crude glycerol concentration, the concentration increasing has a limited effect on single cell internal resistance (Fig. S2) and hydroxyl anion mobility, making glycerol mass transfer the bottle neck of GOR kinetics. Therefore 1.0 M crude glycerol promotes the single cell performance compared to 0.5 M crude glycerol mainly by alleviating glycerol mass transfer issue in the high current density region.

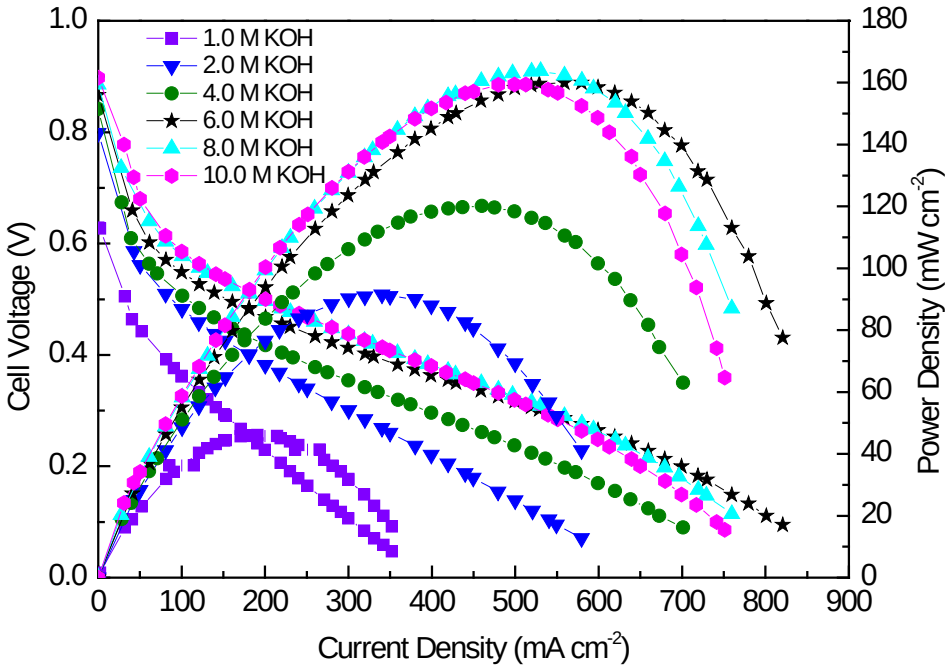

Fig. S3 Polarization and power density curves of direct crude glycerol/O_2 AEMFC with SD-PtCo/CNT as anode catalyst using different KOH concentrations. Anode catalyst (0.5 mg_{Pt} cm^{-2}): SD-PtCo/CNT (Self-prepared); anion exchange membrane: Tokuyama A901; cathode catalyst (3.0 $mg_{catalyst}$ cm^{-2}): Fe-Cu-N_4/C (Acta 4020); anode fuel: 1.0 M crude glycerol, 1.0 ml min^{-1}; cathode fuel: 100 sccm oxygen, ambient pressure; temperature (anode fuel/cathode fuel/cell): 25/60/60 ℃.

As shown in Fig. S3, the cell voltage increases with KOH concentration increasing in the low current density region (<100 mA cm^{-2}). Higher KOH concentration facilitates the dehydrogenation of glycerol's H_α, leading to a higher concentration of alkoxide ion which is an active precursor to aldehyde formation, so that the subsequent elimination of H_β in the anode catalyst layer is enhanced[14].

$$H_\beta R - OH_\alpha \leftrightharpoons H_\beta R - O^- + H_\alpha^+$$

$$H_\beta R - O^- \rightarrow R = O + H_\beta^+ + 2e^-$$

Moreover, higher KOH can neutralize the organic acid generated during the glycerol oxidation process. The local concentration of KOH is thus maintained to a level adequate for continuous oxidation of glycerol. Therefore, higher KOH concentration is favorable toward glycerol oxidation kinetics. It is worth mentioning that the amount of glycerol in the anode catalyst layer is high enough to prevent the system from being limited by mass transfer issue in the low current density region. Based on the above discussion, it can be concluded that higher KOH concentration will boost the single cell performance monotonically in the low current density region.

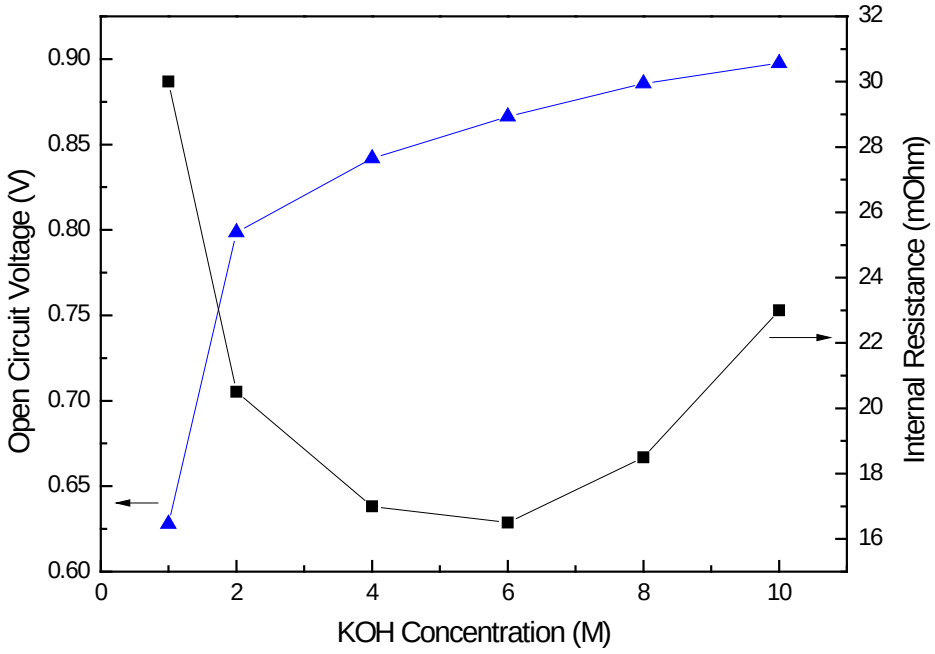

Fig. S4 The effect of KOH concentration on the open circuit voltage and internal resistance.

In the high current density region (>250 mA cm^{-2}), the cell voltage increases with KOH concentration increasing from 0 M to 6.0 M and then decreases with the KOH concentration further increasing from 6.0 M to 10.0 M. This phenomena can be explained by the simultaneous effect of some contrary trends. Higher concentrations of KOH can promote the glycerol oxidation kinetics, as indicated by the rising trend of OCV shown in Fig. S4. A thicker membrane (Tokuyama A201, 28 μm) was adopted in the experiment of AEM based direct ethanol and ethylene glycol fuel cell by Zhao and co-workers.[15, 16] It was found that the internal resistance (IR) is mainly affected by the conduct resistance of hydroxyl anion from cathode side to anode side in the AEM. Hence the single cell IR increases monotonically with KOH concentration rising. However, AEM (Tokuyama A901, 10 μm) adopted in this work is relatively thinner, whereupon the single cell IR is principally dependent on the electric conductivity of the electrolyte. At 60 ℃, the electrical conductivity of the KOH water solution will first increase and then decrease as KOH increases from 0 M to 12.0 M, reaching its maximum value at 6.0-7.0 M[17]. Thereupon, the single cell IR increases as KOH concentration changes from 0 M to 6.0 M and then decreases when KOH concentration further increases from 6.0 M to 10.0 M. Moreover, the adsorption of hydroxyl anion and glycerol is competitive. Too much hydroxyl anion will prevent glycerol from being adequately adsorbed onto the active sites of anode catalyst layer, for the reason that in the high current density region the corresponding consumption rate of glycerol is high. When the KOH concentration increases from 0 M to 6.0 M, the positive effect of internal resistance decline and glycerol oxidation kinetics enhancement surpasses the negative effect of competitive adsorption caused mass transfer issue. When the KOH concentration further increases from 6.0 M to 10.0 M, the negative effect of internal resistance upswing and mass transfer issue will become dominant other than the positive effect of glycerol oxidation kinetics enhancement. In summary, the uptrend of KOH concentration will simultaneously promote and depress the performance for AEM based direct crude glycerol fuel cell.

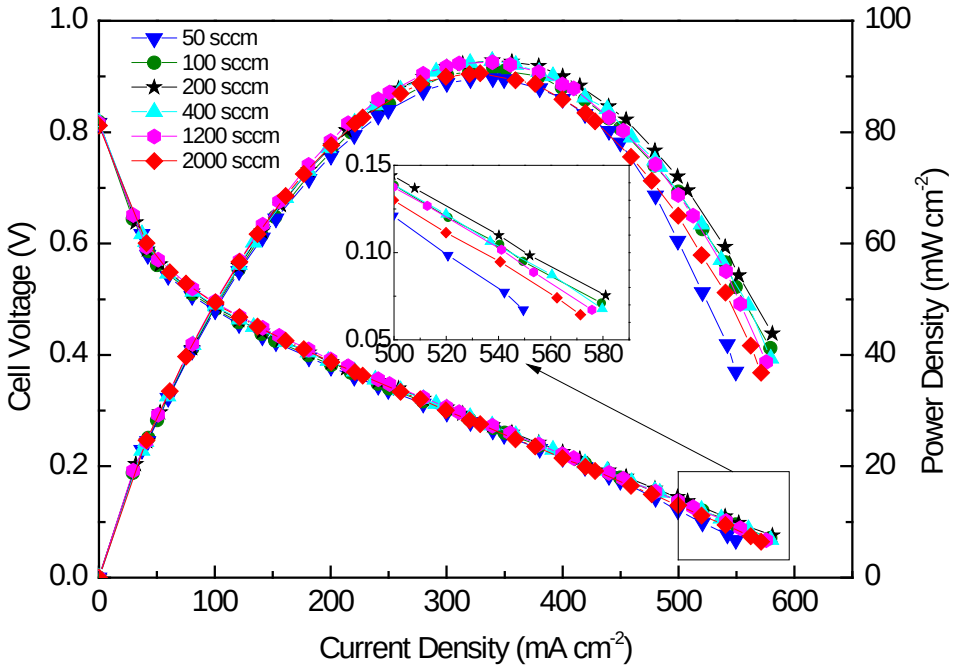

Fig. S5 Polarization and power density curves of direct crude glycerol/O_2 AEMFC with SD-PtCo/CNT as anode catalyst using different cathode oxygen flow rate. Anode catalyst (0.5 mg_{Pt} cm^{-2}): SD-PtCo/CNT (Self-prepared); anion exchange membrane: Tokuyama A901; cathode catalyst (3.0 $mg_{catalyst}$ cm^{-2}): Fe-Cu-N_4/C (Acta 4020); anode fuel: 2.0 M KOH + 1.0 M crude glycerol, 1.0 ml/min; cathode fuel pressure: ambient pressure; temperature (anode fuel/cathode fuel/cell): 25/60/60 ℃.

As shown in Fig. S5, oxygen flow rate has little effect on cell voltage in low current density region. Although not remarkable, it can still be seen that the cell voltage in the mass controlled region will first increase and then decrease with the accretion of oxygen flow rate, indicating the existence of a trade-off between positive effects and negative effects. Higher oxygen flow rate will facilitate its mass transfer, leading to enhanced oxygen reduction reaction (ORR) kinetics so that the single cell performance increases with oxygen flow rate ranging from 50 sccm to 200 sccm. However, the ORR reaction is simultaneously affected by oxygen and water mass transfer due to consumption of water at AEMFC cathode:

$$O_2 + 2H_2O + 4e^- \rightarrow 4OH^-$$

If oxygen flow rate is further increased, water at the cathode will be physically swept out from the cathode catalyst layer. The consequent membrane dryness will deteriorate the water mass transfer for ORR. When the oxygen flow rate increases from 200 sccm to 2000 sccm, the single cell performance will decline in the mass transfer controlled region for the reason that the negative effect of water mass transfer outstrips the positive effect of oxygen mass transfer for ORR.

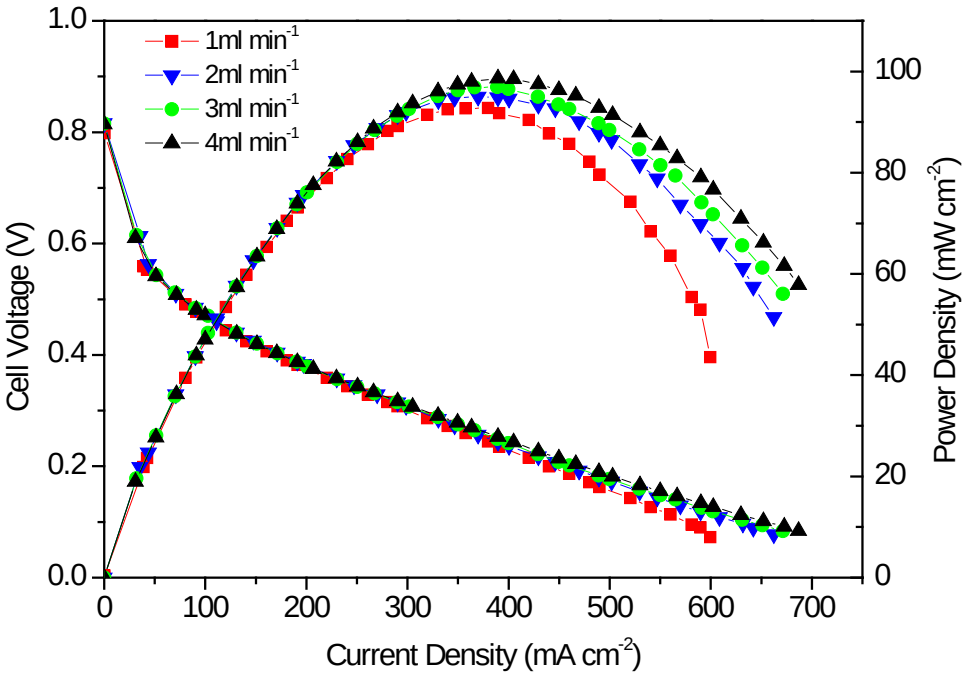

Fig. S6 Polarization and power density curves of direct crude glycerol/O_2 AEMFC with SD-PtCo/CNT as anode catalyst using different anode fuel flow rate. Anode catalyst (0.5 mg_{Pt} cm^{-2}): SD-PtCo/CNT (Self-prepared); anion exchange membrane: Tokuyama A901; cathode catalyst (3.0 $mg_{catalyst}$ cm^{-2}): Fe-Cu-N_4/C (Acta 4020); anode fuel concentration: 2.0 M KOH + 1.0 M crude glycerol; cathode fuel: 100 sccm O_2, ambient pressure; temperature (anode fuel/cathode fuel/cell): 25/60/60 ℃.

Data in Fig. S6 shows no distinct influence of anode fuel flow rate on cell voltage, especially in the low current region. In the high current density region, higher glycerol and KOH consumption rate will be compensated by better mass transfer of glycerol and hydroxyl anion in the anode catalyst layer as a result of higher fuel flow rate, which can be regarded as the reason for the slight increase of single cell performance.

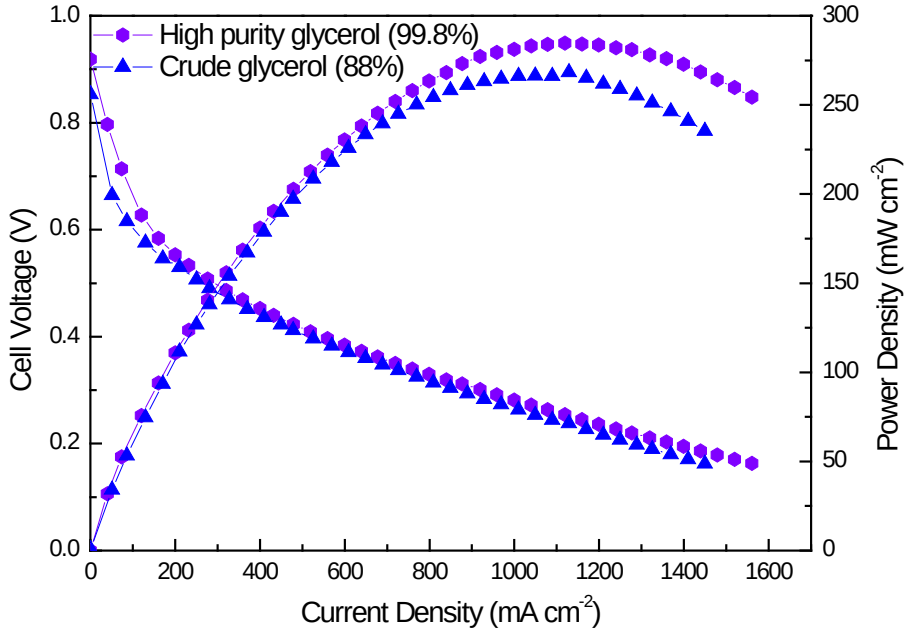

Fig. S7 Polarization and power density curves of direct crude glycerol/O_2 AEMFC with SD-PtCo/CNT as anode catalyst using high purity and crude glycerol. Anode catalyst (0.5 mg_{Pt} cm^{-2}): SD-PtCo/CNT (Self-prepared); anion exchange membrane: Tokuyama A901; cathode catalyst (3.0 $mg_{catalyst}$ cm^{-2}): Fe-Cu-N_4/C (Acta 4020); electrolyte concentration: anode fuel concentration: 6.0 M KOH+3.0 M high purity & crude glycerol; anode fuel flow rate: 4.0 ml min^{-1}; cathode fuel flow rate: 200 sccm O_2, ambient pressure; temperature (anode fuel/cathode fuel/cell): 25/80/80 ℃.

The cell voltage of high purity glycerol based AEMFC is slightly higher than that of crude glycerol based AEMFC, which is attributed to some impurities in the crude glycerol. The peak power density of high purity glycerol based AEMFC (284.6 mW cm^{-2}) is only 16.1 mW cm^{-2} higher than that of crude glycerol based AEMFC (268.5 mW cm^{-2}), revealing that the impurities in crude glycerol do not have remarkable effect on glycerol's adsorption on the anode catalyst active sites.

Comparison of glycerol oxidation on SD-PtCo/CNT, Pt/CNT, Pt/C in three-electrode one-compartment cell

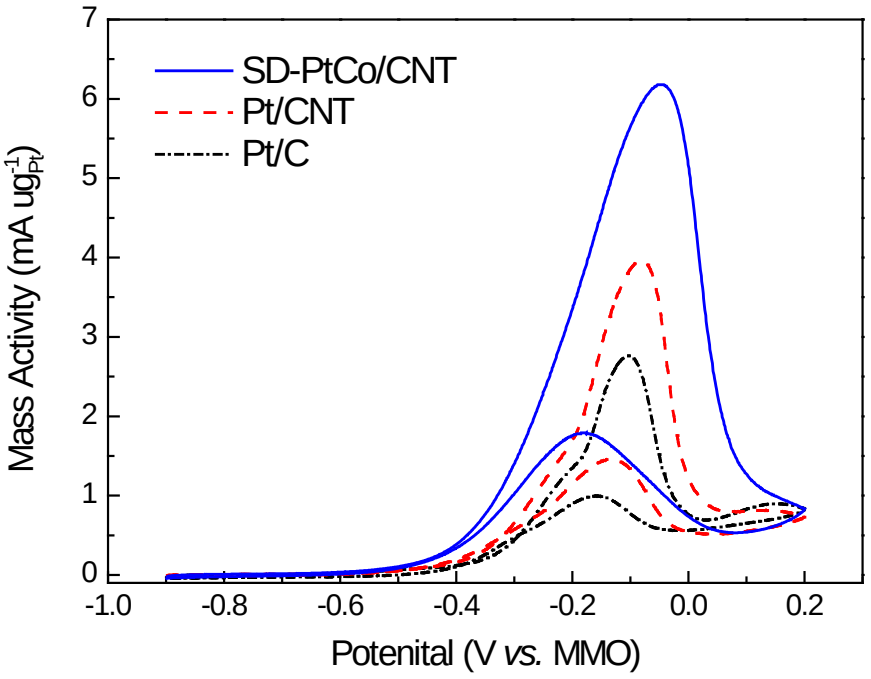

Fig. S8 Cyclic voltamgrams of Pt/C, Pt/CNT and SD-PtCo/CNT for glycerol oxidation in N_2 purged 2.0 M KOH + 1.0 M glycerol at 50 mV s^{-1}, room temperature.

Although the Pt/C catalyst has a smaller particle size, the network structure of Pt/CNT catalyst layer in three dimensional space[18] offers more active sites, better glycerol and hydroxyl anion mass transfer and electron transfer than Pt/C does. Consequently, the onset potential of glycerol oxidation on Pt/CNT is 50 mV more negative than that of Pt/C while the peak current mass activity of Pt/CNT is 1.20 mA μg^{-1} higher than that of Pt/C. As discussed in the article, the SD-PtCo/CNT prepared by the dealloy technique facilitates the rate determining step (RDS) of glycerol oxidation and enlarge the catalyst ECSA, thus accelerating the glycerol oxidation reaction rate. Consequently, the onset potential of glycerol oxidation on SD-PtCo/CNT is 100 mV more negative than that of Pt/CNT, while the peak current mass activity of SD-PtCo/CNT is 2.22 mA μg^{-1} higher than that of Pt/CNT.

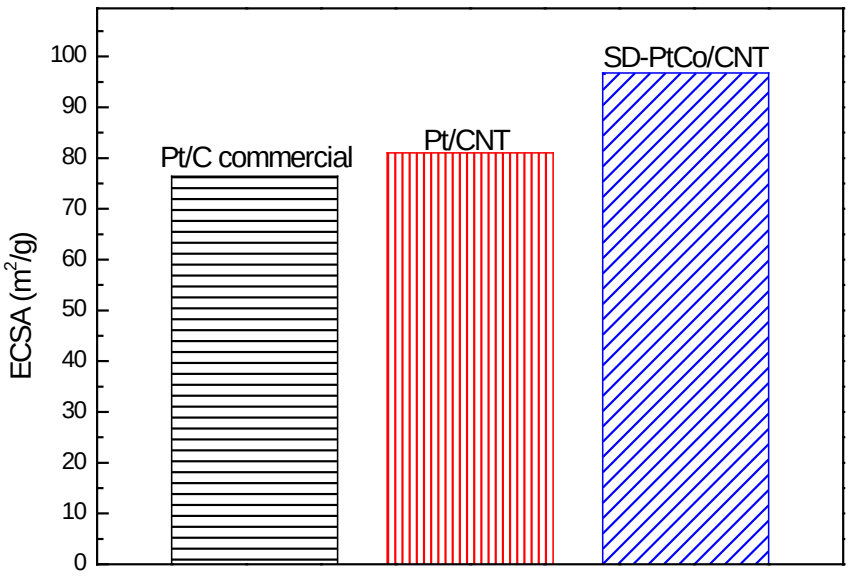

Fig. S9 Comparison of electrochemically active area (ECSA) calculated from platinum reduction peak (For poly polycrystalline Pt electrode, its oxide reduction process has a pseudo-capacity of 0.440 mC cm^{-2})[19] obtained on Pt/C, Pt/CNT and SD-PtCo/CNT in 1.0 M KOH at 50 mV s^{-1}, room temperature. The scan range is from -0.9 V to 0.4 V *vs.* MMO.

Although the particle size of Pt/CNT (2.9 nm) is larger than that of Pt/C (1.8 nm) according to XRD results, its ECSA is still larger than that of Pt/C, which can be attributed to the higher exposure level of Pt particles offered by the three dimensional network catalyst layer.[18] The ECSA of SD-PtCo/CNT (97 m^2/g) is higher than that of Pt/CNT (81 m^2/g) , which is due to surface roughness and smaller particle size of Pt particles.

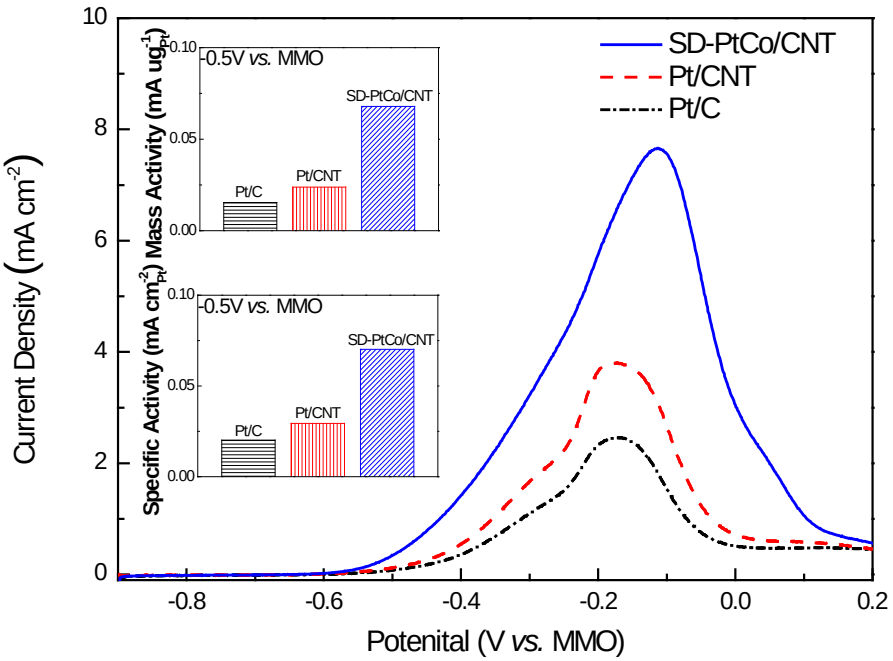

Fig. S10 Linear scan voltammograms of of Pt/C, Pt/CNT and SD-PtCo/CNT for glycerol oxidation in N_2 purged 2.0 M KOH + 1.0 M glycerol at 1 mV s^{-1}, room temperature.

The onset potential, peak current density, mass activity at and specific activity at -0.5 V shown in Fig. S10 indicate that the catalyst activity toward glycerol oxidation is SD-PtCo/CNT > Pt/CNT > Pt/C, which is consistent with results of half cell fast CV scan and single cell performance. For Pt/CNT, the combine effect of its larger ECSA and higher specific activity as a result of enhanced mass transfer of glycerol and OH^- leads to its higher mass activity than Pt/C. For SD-PtCo/CNT, its ECSA is further enlarged while its specific activity is improved by d-band center shift owing to compressed lattice and optimized electronic properties tuned by the sub-layer transitional metal atoms, resulting in much higher mass activity than both Pt/CNT and Pt/C.

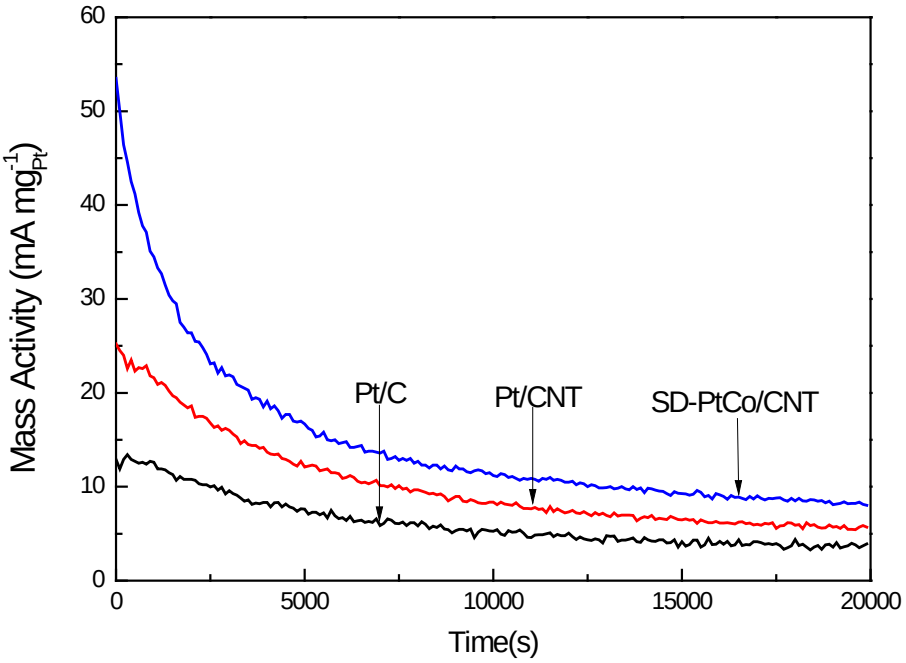

Fig. S11 Chronoamperometic profiles of of Pt/C, Pt/CNT and SD-PtCo/CNT for glycerol oxidation in 2.0 M KOH and 1.0 M glycerol at 1 mV s^{-1}, room temperature.

The chronoamperometry on these catalysts in Fig. S11 was also obtained at the applied voltage of -0.5 V (*vs.* MMO) also to compare their reaction stability towards glycerol oxidation. The applied voltage was held for 20000 seconds to obtain a pseudosteady state current density profile. At 20000 seconds, the pseudosteady state mass activity is in the order: SD-PtCo/CNT > Pt/CNT > Pt/C, indicating that the long-term activity towards glycerol oxidation has been improved by employing SD-PtCo/CNT.

Fuel conversion and efficiency analysis

$$Fuel\ conversion = \frac{C_0 - C_f}{C_0}$$

C_0 is the concentration of glycerol supplied to the single cell chamber, while C_f, quantified by HPLC, is the concentration of glycerol coming out of the single cell chamber.

$$Fuel\ effciency = \frac{Q_{actual}}{Q_{total}} = \frac{\int_{t_0}^{t_f} Idt}{nmF}$$

Q_{actual} is the actual charge passing through the external circuit, while Q_{total} is the theoretical charge generated by supplied glycerol assuming a complete oxidation product of CO_2. t_0 and t_f is the reaction start and stop time, respectively. I is the current of external circuit recorded by the fuel cell test stand. n equals 14 as the complete oxidation product is CO_2. m is the total mole amount of glycerol supplied between t_0 and t_f. F is the Faraday constant (96485.33 C mol^{-1}).

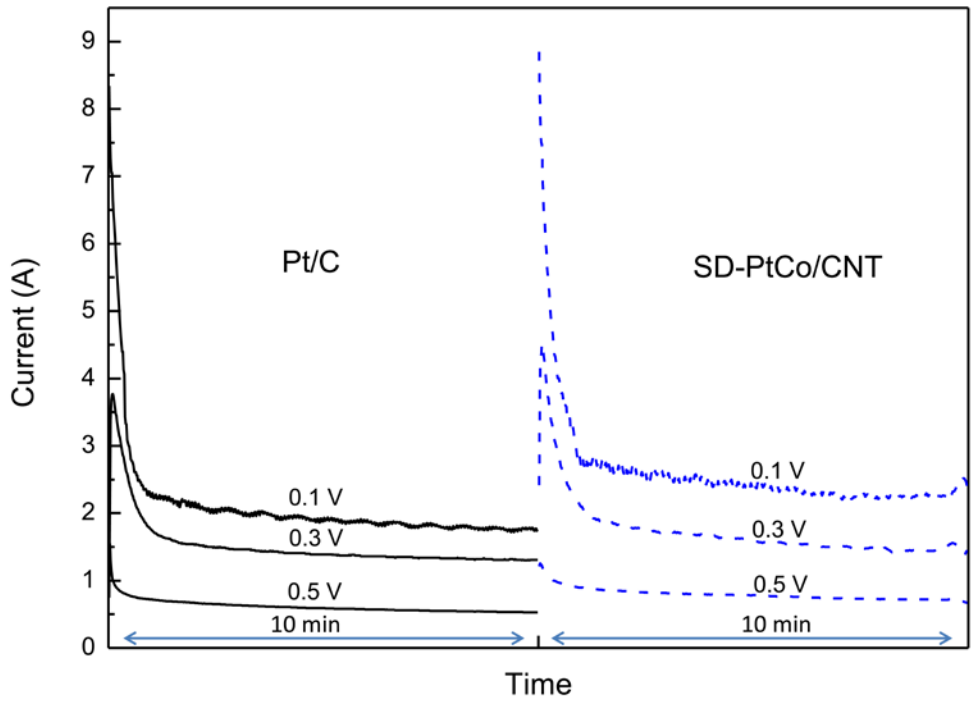

Fig. S12 Transient cell current of the direct glycerol fuel cell with Pt/C or SD-PtCo/CNT as anode catalyst at different cell voltages. AEM: Tokuyama A901; cathode catalyst: Fe-Cu-N_4/C (Acta 4020), 3.0 $mg_{catalyst}$ cm^{-2}; anode fuel: 6.0 M KOH + 1.0 M high purity glycerol (99.8 wt%), 1.0 ml min^{-1}; cathode fuel: 100 sccm O_2, ambient pressure; temperature (anode fuel/cathode fuel/cell): 25/60/60 °C.

Tab. S2 Comparison of fuel conversion and efficiency on Pt/C and SD-PtCo/CNT anode catalysts at 60 ^{o}C.

Catalyst	Cell Voltage (V)	Fuel Conversion	Fuel Efficiency
Pt/C	0.5	7.94 %	2.60 %
Pt/C	0.3	13.87 %	6.14 %
Pt/C	0.1	19.14 %	8.39 %
SD-PtCo/CNT	0.5	12.64 %	3.40 %
SD-PtCo/CNT	0.3	20.82 %	7.02 %
SD-PtCo/CNT	0.1	27.30 %	10.53 %

OA: oxalate, LA: lactate, GA: glycerate, TA: tartronate, MA: mesoxalate

When the current was steady (from 3 min to 8 min), the fuel solution was collected for HPLC analysis to determine converted glycerol. As shown in Fig. S12, the single cell with the SD-PtCo/CNT anode catalyst generates higher current than the one with Pt/C does at each operating cell voltage, which is consistent with the results of half cell CV test and single cell scan current test. Higher current indicates that more electrons are taken out of certain amount of provided glycerol. As a result, the fuel conversion and fuel efficiency of the single cell with the SD-PtCo/CNT anode catalyst is higher than those of single cell with Pt/C anode catalyst. Therefore, SD-PtCo/CNT can be used as efficient anode catalyst with enhanced fuel utilization, which is fairly high for active AEM based direct glycerol fuel cell.

State-of-the-art of direct glycerol fuel cells

Tab. S3 State-of-the-art of direct glycerol fuel cells based on the relationship between peak power density and operating temperature.

Fuel cell type	Fuel	Anode catalyst	Cathode catalyst	Electrolyte	Operating temperature (°C)	*PPD (mW cm^{-2})	Mass activity (**Unit)	Ref
SOFC	Glycerol/water(1:3)	Ni	LSM	8YSZ	650 750 800	125 225 265	-	20
SOFC	High purity glycerol	Ni on LSFCO	CGO	LSFCO-CGO	800	327	-	3, 21, 22
SOFC	Glycerol/water(50wt%)	LNCO-NSDC	LNCO-NSDC	NSDC	580	215	-	4
AEMFC	6.0 M KOH 3.0 M Crude & High purity glycerol	SD-PtCo/CNT 0.5 mg_{Pt} cm^{-2}	Fe-Cu-N_4/C	Tokuyama A901	80	268.5 (Crude glycerol) 284.6 (High purity glycerol)	537 569.2	(This work)
AEMFC	2.0 M KOH 1.0 M Crude glycerol	SD-PtCo/CNT 0.5 mg_{Pt} cm^{-2}	Fe-Cu-N_4/C	Tokuyama A901	25 40 60 80	35.5 52.5 91.5 141.4	71 105 183 282.8	(This work)
AEMFC	1.0 M Glycerol 2.0 M KOH	Pt/C 1.0 mg_{Pt} cm^{-2}	Fe-Cu-N_4/C	Tokuyama A201	50 80	58.6 124.5	58.6 124.5	2
AEMFC	Glycerol (5%wt) 2.0 M KOH	Pd-(Ni-Zn)/C 1.0 mg_{Pd} cm^{-2}	Fe-Co/C	Tokuyama A-006	22 80	24 100	24 100	23
AEMFC	1.0 M Glycerol 2.0 M KOH	Au/C 1.0 mg_{Au} cm^{-2}	Fe-Cu-N_4/C	Tokuyama A201	50 60 70 80	17.5 26.3 37.1 57.9	17.5 26.3 37.1 57.9	24
AEMFC	Glycerol (5%wt) 2.0 M KOH	Pd/CNT 1.0 mg_{Pd} cm^{-2}	Fe-Co/C	Tokuyama A-006	25 40 60 80	18 32 54 79	18 32 54 79	25
AEMFC	Glycerol (25%wt) 3.0 M KOH	Pt-Ru/C 0.5 mg_{Pt} cm^{-2}	Pt/C 0.5 mg_{Pt} cm^{-2}	eVionyx Tokuyama Asahi Glass Co.	25	4.3	8.6	26
AEMFC	1.0 M Glycerol 6.0 M KOH	Pt/C 1 mg_{Pt} cm^{-2}	Pt/C 2 mg_{Pt} cm^{-2}	ADP	60	25	8.3	27
AEMFC	.01 M Glycerol 1.0 M KOH	PtRu/C 4 $mg_{Pt\text{-}Ru}$ cm^{-2}	Pt/C 1 mg_{Pt} cm^{-2}	Tokuyama AHA	50	6.8	1.16	28

MFC	Crude glycerol Phosphate buffer solution	-	Pt/C 0.35 mg_{Pt} cm^{-2}	-	25	0.211	0.63	29
MFC	Glycerol Phosphate buffer solution	Rhodopseudomonas palustris DX-1	Pt/C 0.5 mg_{Pt} cm^{-2}	-	25	0.272	0.544	30
MFC	Glycerol Phosphate buffer solution	PQQ-ADH PQQ-AldDH	Pt/C	Nafion NRE212	25	1.32	-	31
MFC	Glycerol Phosphate buffer solution	PQQ-ADH PQQ-AldDH	Pt/C	TMOA modified Nafion	25	1.21	-	32
MFC	Glycerol Phosphate buffer solution	BBK006	Pt Wire	FAA	25	0.006	-	33

*PPD: Peak power density

**Unit: mW $mg_{precious\ metal\ per\ MEA}^{-1}$

AEMFC: Anion exchange membrane fuel cell

SOFC: Solid oxide fuel cell

References

01 New uses make refined glycerine oleochem leader, http://www.icis.com/Articles/2012/01/04/9517016/outlook-12-new-uses-make-refined-glycerine-oleochem-leader.html, Accessed 01-24, 2012.

02 Z. Zhang, L. Xin and W. Li, *Appl. Catal., B*, 2012, **119-120**, 40-48.

03 M. Lo Faro, M. Minutoli, G. Monforte, V. Antonucci and A. S. Aricò, *Biomass and Bioenergy*, 2011, **35**, 1075-1084.

04 H. Qin, Z. Zhu, Q. Liu, Y. Jing, R. Raza, S. Imran, M. Singh, G. Abbas and B. Zhu, *Energy & Environmental Science*, 2011, **4**, 1273-1276.

05 Methanex Regional Posted Contract Prices, http://www.methanex.com/products/methanolprice.html, Accessed 11-24, 2012.

06 G. K. S. Prakash, F. C. Krause, F. A. Viva, S. R. Narayanan and G. A. Olah, *J. Power Sources* 2011, **196**, 7967-7972.

07 A. S. Aricò, P. Cretì, E. Modica, G. Monforte, V. Baglio and V. Antonucci, *Electrochim. Acta* 2000, **45**, 4319-4328.

08 S. A. Kuliyev, S. Aksongur, M. D. Mat, B. Ibrahimoğlu and M. D. Kozlu, *ECS Trans.* , 2009, **25**, 1093-1098.

09 Ethanol TFC Commodity Charts, http://futures.tradingcharts.com/chart/AC/W, Accessed 11-24, 2012.

10 J. B. Xu, T. S. Zhao, Y. S. Li and W. W. Yang, *Int. J. Hydrogen Energy* 2010, **35**, 9693-9700.

11 L. An, T. S. Zhao, R. Chen and Q. X. Wu, *J. Power Sources* 2011, **196**, 6219-6222.

12 L. Jiang, G. Sun, S. Sun, J. Liu, S. Tang, H. Li, B. Zhou and Q. Xin, *Electrochim. Acta* 2005, **50**, 5384-5389.

13 S. Song and P. Tsiakaras, *Appl. Catal., B* 2006, **63**, 187-193.

14 Y. Kwon, S. C. S. Lai, P. Rodriguez and M. T. M. Koper, *J. Am. Chem. Soc.* , 2011, **133**, 6914-6917.

15 Y. S. Li, T. S. Zhao and Z. X. Liang, *J. Power Sources* 2009, **187**, 387-392.

16 L. An, T. S. Zhao, S. Y. Shen, Q. X. Wu and R. Chen, *Int. J. Hydrogen Energy* 2010, **35**, 4329-4335.

17 R. J. Gilliam, J. W. Graydon, D. W. Kirk and S. J. Thorpe, *Int. J. Hydrogen Energy* 2007, **32**, 359-364.

18 G. Gao and C. D. Vecitis, *ACS Applied Materials & Interfaces*, 2012.

19 B. E. Conway, *Prog. Surf. Sci.* , 1995, **49**, 331-452.

20 J. Y. Won, H. J. Sohn, R. H. Song and S. I. Woo, *ChemSusChem*, 2009, **2**, 1028-1031.

21 M. Lo Faro, D. La Rosa, M. Minutoli, G. Monforte, V. Antonucci and A. S. Aricò, *ECS Trans.* , 2009, **25**, 2241-2248.

22 M. Lo Faro, A. Stassi, G. Monforte, M. Minutoli, V. Antonucci, V. Modafferi, P. Frontera, C. Busacca, P. Antonucci and A. S. Aricò, *ECS Trans.* , 2011, **35**, 1753-1760.

23 V. Bambagioni, M. Bevilacqua, J. Filippi, A. Marchionni, S. Moneti, F. Vizza and C. Bianchini, *Chimica Oggi*, 2010, **28**, VII-X.

24 Z. Zhang, L. Xin and W. Li, *International Journal of Hydrogen Energy*, 2012, **37**, 9393-9401.

25 V. Bambagioni, C. Bianchini, A. Marchionni, J. Filippi, F. Vizza, J. Teddy, P. Serp and M. Zhiani, *Journal of Power Sources*, 2009, **190**, 241-251.

26 S. R. Ragsdale and C. B. Ashfield, *ECS Transactions*, 2008, **16**, 1847-1854.

27 A. Ilie, M. Simoes, S. Baranton, C. Coutanceau and S. Martemianov, *Journal of Power Sources*, 2011, **196**, 4965-4971.

28 K. Matsuoka, Y. Iriyama, T. Abe, M. Matsuoka and Z. Ogumi, *Journal of Power Sources*, 2005, **150**,

27-31.

29 Y. Feng, Q. Yang, X. Wang, Y. Liu, H. Lee and N. Ren, *Bioresource Technology*, 2011, **102**, 411-415.

30 D. Xing, Y. Zuo, S. Cheng, J. M. Regan and B. E. Logan, *Environmental Science & Technology*, 2008, **42**, 4146-4151.

31 R. L. Arechederra and S. D. Minteer, *Fuel Cells (Weinheim, Ger.)*, 2009, **9**, 63-69.

32 R. L. Arechederra, B. L. Treu and S. D. Minteer, *Journal of Power Sources*, 2007, **173**, 156-161.

33 V. R. Nimje, C.-Y. Chen, C.-C. Chen, H.-R. Chen, M.-J. Tseng, J.-S. Jean and Y.-F. Chang, *Bioresource Technology*, 2011, **102**, 2629-2634.